EPR Definition of the Non-Heme Ferric Active Sites of Mammalian 15-Lipoxygenase: Major Spectral Difference Relative to Human 5-Lipoxygenases and Plant Lipoxygenases and Their Ligand Field Origin

Yan Zhang,[†] Qing-Fen Gan,[†] Elizabeth G. Pavel,[‡] Elliott Sigal,[†] and Edward I. Solomon*,[‡]

Contribution from the Institute of Biochemistry and Cell Biology, Syntex Discovery Research, Palo Alto, California 94304, and the Department of Chemistry, Stanford University, Stanford, California 94305

Received September 20, 1994[⊗]

Abstract: Lipoxygenases (LOs) are non-heme iron containing enzymes which catalyze the hydroperoxidation of polyunsaturated fatty acids. Mammalian LOs have great physiological and pathological importance as they play key roles in the biosynthesis of leukotrienes and lipoxins. Electron paramagnetic resonance (EPR) studies have shown that ferric active sites of soybean lipoxygenase-1 (SLO-1) and human 5-lipoxygenase (5-HLO) exhibit axial EPR patterns which convert to rhombic spectra upon addition of hydroperoxide product (13-HPOD). In this report, we extend EPR studies to rabbit (15-RLO) and human (15-HLO) mammalian 15-LOs. The spectra of 15-RLO and 15-HLO have rhombic high-spin ferric EPR signals which convert to axial upon interaction with product, opposite to the behavior reported for SLO-1 and 5-HLO, which is indicative of a significant structural difference between the ferric sites of these mammalian 15-LOs and those of SLO-1 and 5-HLO. This appears to relate to the substitution of an asparagine ligand in the SLO-1 and 5-HLO active sites for a histidine ligand in the rabbit and human 15-LOs. A ligand field model of the zero-field splitting is presented which accounts for this opposite EPR spectral behavior in terms of ligand strength differences associated with the Asn (weak) → His (strong) ligand substitution.

Introduction

Lipoxygenases (LOs) are a class of non-heme iron containing enzymes which catalyze the dioxygenation of polyunsaturated fatty acids which contain one or more 1,4-*cis*,*cis*-pentadiene units to yield hydroperoxide products. LOs are found in both plants and animals. Mammalian LOs have great physiological and pathological importance as they play key roles in the biosynthesis of leukotrienes and lipoxins.[1] In mammals, 5-, 12-, and 15-LOs are distinguished by their insertion of dioxygen at the indicated carbon position of arachidonic acid. LOs contain one iron atom per molecule, and the iron has been identified as the center of enzymatic activity. The iron in the isolated resting form of LOs is in the ferrous oxidation state and must be oxidized to the ferric state to activate the enzyme.

Ferrous soybean lipoxygenase-1 (SLO-1, a 15-lipoxygenase) has been studied by various spectroscopic techniques which have suggested that the active site geometry is five- and/or six-coordinate distorted octahedral.[2-7] Two X-ray crystal structures have been reported: Boyington *et al.* have described the iron active site as four-coordinate,[8] while Minor *et al.* have identified five ligands.[9] Recent low-temperature crystallographic results by Minor *et al.* to 1.6-Å resolution suggest that water is also a ligand,[10] bringing the total coordination number to six. In terms of amino acid ligands to the iron, the two published structures have identified His_{499}, His_{504}, His_{690}, and Ile_{839} (through the C-terminus carboxylate) as residues coordinated to the active site iron. The Asn_{694} residue is also found to be a ligand in the Minor *et al.* structure with a relatively long bond length. Of these ligating amino acids, the three histidine residues and C-terminal isoleucine are conserved in all sequenced LOs.[11] The asparagine is also conserved with few exceptions;[12-15] these exceptions include rabbit and human 15-lipoxygenases where this asparagine is substituted by histidine.[16,17] It is important to note that human 5-lipoxygenase (5-HLO) does not have this substitution.[11]

[†] Institute of Biochemistry and Cell Biology, Syntex Discovery Research.
[‡] Stanford University.
[⊗] Abstract published in *Advance ACS Abstracts*, June 15, 1995.

(1) Samuelsson, B.; Dahlén, S.-E.; Lindgren, J. A.; Rouzer, C. A.; Serhan, C. N. *Science* **1987**, *237*, 1171.
(2) Dunham, W. R.; Carroll, R. T.; Thompson, J. F.; Sands, R. H.; Funk, M. O., Jr. *Eur. J. Biochem.* **1990**, *190*, 611.
(3) Feiters, M. C.; Boelens, H.; Veldink, G. A.; Vliegenthart, J. F. G.; Navrataram, S.; Allen, J. C.; Nolting, H.-F.; Hermes, C. *Recl. Trav. Chim. Pays-Bas* **1990**, *109*, 133.
(4) Scarrow, R. C.; Trimitsis, M. G.; Buck, C. P.; Grove, G. N.; Cowling, R. A.; Nelson, M. J. *Biochemistry* **1994**, *33*, 15023.
(5) Whittaker, J. W.; Solomon, E. I. *J. Am. Chem. Soc.* **1988**, *110*, 5329.
(6) Pavlosky, M. A.; Solomon, E. I. *J. Am. Chem. Soc.* **1994**, *116*, 11610.
(7) Pavlosky, M. A.; Zhang, Y.; Westre, T. E.; Gan, Q.-F.; Pavel, E. G.; Campochiaro, C.; Hedman, B.; Hodgson, K. O.; Solomon, E. I. *J. Am. Chem. Soc.* **1995**, *117*, 4316.
(8) Boyington, J. C.; Gaffney, B. J.; Amzel, L. M. *Science* **1993**, *260*, 1482.
(9) Minor, W.; Steczko, J.; Bolin, J. T.; Otwinowski, Z.; Axelrod, B. *Biochemistry* **1993**, *32*, 6320.
(10) Minor, W.; Bolin, J. T.; Axelrod, B., personal communication.
(11) Sloane, D. L. In *Lipoxygenases and Lipoxygenase Pathway Enzymes;* AOCS Press: Champaign, IL, 1995.
(12) Chen, X.-S.; Kurre, U.; Jenkins, N. A.; Copeland, N. G.; Funk, C. D. *J. Biol. Chem.* **1994**, *269*, 13979.
(13) Watanabe, T.; Medina, J. F.; Haeggström, J. Z.; Rådmark, O.; Samuelsson, B. *Eur. J. Biochem.* **1993**, *212*, 605.
(14) DeMarzo, N.; Sloane, D. L.; Dicharry, S.; Highland, E.; Sigal, E. *Am. J. Physiol.* **1992**, *262*, L198.
(15) Yoshimoto, T.; Suzuki, H.; Yamamoto, S.; Takai, T.; Yokoyama, C.; Tanabe, T. *Proc. Natl. Acad. Sci. U.S.A.* **1990**, *87*, 2142.
(16) Sigal, E.; Craik, C. S.; Highland, E.; Grunberger, D.; Costello, L. L.; Dixon, R. A. F.; Nadel, J. A. *Biochem. Biophys. Res. Commun.* **1988**, *157*, 457.
(17) Fleming, J.; Thiele, B. J.; Chester, J.; O'Prey, J.; Janetzki, S.; Aitken, A.; Anton, I. A.; Rapoport, S. M.; Harrison, P. R. *Gene* **1989**, *79*, 181.

0002-7863/95/1517-7422$09.00/0

Extended X-ray absorption fine structure (EXAFS)[4] and magnetic circular dichroism (MCD)[18] studies have described the ferric SLO-1 active site as six-coordinate with hydroxide[4] as the sixth ligand, and electron paramagnetic resonance (EPR) isotope studies support the presence of a water-based ligand.[19] Ferric active sites of SLO-1 and 5-HLO have also been studied by EPR and absorption spectroscopies.[18,20,21] Both ferric SLO-1 and 5-HLO exhibit multicomponent axial EPR patterns with dominant signals centered in the $g = 6$ region and an optical absorption band at 350 nm. The axial EPR signal of SLO-1 converts to a rhombic signal at $g = 4.3$ upon addition of >1 equiv of the hydroperoxide product, 13-(*S*)-hydroperoxy-9,11-(*E,Z*)-octadecadienoic acid (13-HPOD).[20,22] This EPR conversion is also associated with the growth of an absorption band at 580 nm (*i.e.*, formation of the purple form). It was suggested that product is directly bound to the iron and that the purple color of this ferric−product complex is due to a peroxide→Fe^{3+} charge transfer transition.[18,23]

The non-heme ferric active site is high-spin d^5 with a $^6A_1$ ground state that undergoes zero-field splitting (ZFS) according to the spin Hamiltonian in eq 1, where D is the axial and E is

$$\mathcal{H} = D[S_z^2 - S(S+1)/3] + E(S_x^2 - S_y^2) \qquad (1)$$

the rhombic ZFS parameter. For axial complexes ($E/D \approx 0$), solution of the spin Hamiltonian gives three doublets, $M_S = \pm 1/2, \pm 3/2, \pm 5/2$, which are split by $2D$ and $4D$, respectively. In this case, an axial EPR signal arises from the $M_S = \pm 1/2$ doublet with $g_{\parallel} = 2.0$ and $g_{\perp} = 6.0$. For complexes at the rhombic limit ($E/D = 1/3$), three equally spaced doublets, separated by an amount $Z = 3.5D$, are obtained. A large EPR signal is derived from the middle doublet as it has an isotropic g-value of ~4.3; there is also a weak highly anisotropic signal for the lower doublet with one g-value of ~9.6 and two of ~0.7. The doublet splitting, and therefore the ZFS parameter D, can be obtained through the temperature dependence of the EPR signal, and the E/D ratio is obtained from the ground-state g-values. Variable-temperature MCD and EPR spectroscopies have been used to obtain the ZFS parameters of the ferric SLO-1 active site, and the relation of these spin Hamiltonian parameters to molecular properties has been developed using ligand field (LF) theory.[18]

In this study, dramatically different EPR behavior is observed for the oxidized rabbit reticulocyte 15-lipoxygenase (15-RLO) and human recombinant 15-lipoxygenase (15-HLO) relative to SLO-1 and 5-HLO, which is thus indicative of a significant structural difference between the ferric site of these mammalian 15-LOs and those of SLO-1 and 5-HLO. We have applied a LF analysis of the ZFS parameters[18] to the mammalian LO systems to gain insight into the observed opposite EPR spectral behavior in terms of ligand field differences associated with a possible Asn→His ligand substitution.

Experimental Section

15-RLO was isolated from 55% ammonium sulfate precipitate of rabbit reticulocytes, with specific activity of ~15 unit/μg (unit = mM product/min), according to previously published procedures.[24] The 15-RLO used for EPR studies was in 10 mM bis-Tris, 0.2 M NaCl, pH = 6.8 buffer. 15-HLO was purified from a baculovirus/insect cell expression system as described earlier.[25] Purified 15-HLO was concentrated and buffer exchanged into 20 mM phosphate, 0.2 M NaCl, pH = 7.0 buffer using an Amicon concentrator with a YM30 membrane. The specific activity of 15-HLO was 5−10 units/μg. The specific activities of 15-RLO and 15-HLO are comparable to or higher than the maximal values reported.[25,26] The metal content was determined by atomic absorption analysis using a Perkin-Elmer Model 2380 graphite furnace AA spectrometer. The average iron content was 70 ± 10% Fe/enzyme for 15-RLO and 55 ± 10% Fe/enzyme for 15-HLO. The native enzyme was treated with 13-HPOD to produce the ferric forms for EPR studies. 13-HPOD was purchased from Oxford Biochemical Research and added to the enzymes after the ethanol solvent had been evaporated. Addition of a stoichiometric amount of product to both enzymes did not decrease their specific activity.

EPR spectra were obtained on a Bruker ER 220-D SRC spectrometer, equipped with a Lake Shore cryotronics temperature controller Model DTC-500 and an Air Products Liquid Transfer Heli-Tran Refrigerator dewar. The temperature was measured with a carbon glass resistor mounted in a EPR tube. The UV/vis absorption spectra were recorded on a Hewlett Packard HP 8452A diode array spectrophotometer at room temperature. The amount of EPR-visible iron in an enzyme sample was determined by EPR quantitation against a ferric EDTA standard. Fe(III)EDTA was prepared by the addition of excess sodium EDTA to ferric chloride in a 50% glycerol solution. The EPR spectra of 15-RLO and ferric EDTA standards for spin quantitation were recorded at 7.8 K with microwave power of 1.01 mW and modulation amplitudes of 20 and 10 G, respectively. EPR parameters for the 15-RLO spectra shown were as follows: temperature, 7 K; microwave frequency, 9.52 GHz; power, 10.1 mW; modulation amplitude 20 G; gain, 3.2×10^4. The EPR parameters for the 15-HLO spectra shown were as follows: temperature, 7 K; microwave frequency, 9.52 GHz; power, 10.1 mW; modulation amplitude 12.5 G; gain, 2.5×10^4. Spin quantitation and temperature dependence data were collected under non-power-saturation conditions which were determined by power *vs* intensity tests. The intensity factor g_p^{av} was calculated using eq 6 of Aasa and Vänngård.[27] To account for the thermal population of the three Kramers doublets, ZFS parameters were determined by measuring the temperature dependence of the EPR amplitude since the line width of the EPR signal did not appear to broaden in the temperature range used. The ZFS parameters obtained were used to determine the Boltzmann population of each doublet. The program SIM 15[28] was used to simulate 15-RLO EPR spectra for spin quantitation purposes.

Results and Analysis

The EPR spectrum of resting 15-RLO isolated from rabbit reticulocytes is mainly EPR-silent, as shown in Figure 1a, indicating that the iron is in the reduced ferrous form even in air, which is consistent with results on other LOs.[20,21] The observed sharp EPR signals positioned at $g = 6$ and 6.5 are due to a small amount of heme contaminant present in the sample.[29] Addition of 13-HPOD hydroperoxide product to ferrous 15-RLO results in an EPR signal at $g = 4.3$ which is proportional to the amount of 13-HPOD used up to 1 equiv, indicating that the ferrous center in the active site has been oxidized to the EPR-active ferric form. The EPR spectrum of

(18) Zhang, Y.; Gebhard, M. S.; Solomon, E. I. *J. Am. Chem. Soc.* **1991**, *113*, 5162.
(19) Nelson, M. J. *J. Am. Chem. Soc.* **1988**, *110*, 2985.
(20) Veldink, G. A.; Vliegenthart, J. F. G. *Adv. Inorg. Biochem.* **1984**, *6*, 139.
(21) Chasteen, N. D.; Grady, J. K.; Skorey, K. I.; Neden, K. J.; Riendeau, D.; Percival, M. D. *Biochemistry* **1993**, *32*, 9763.
(22) There is one report of SLO-1 not converting to the purple form when treated with >1 equiv of product (Pistorius *et al. J. Biol. Chem.* **1976**, *251*, 7144).
(23) Zang, Y.; Elgren, T. E.; Dong, Y.; Que, L., Jr. *J. Am. Chem. Soc.* **1993**, *115*, 811.
(24) Gan, Q.-F.; Witkop, G. L.; Sloane, D. L.; Straub, K. M.; Sigal, E. *Biochemistry* **1995**, *34*, 7069.
(25) Kühn, H.; Barnett, J.; Grunberger, D.; Baecker, P.; Chow, J.; Nguyen, B.; Bursztyn-Pettegrew, H.; Chan, H.; Sigal, E. *Biochim. Biophys. Acta* **1993**, *1169*, 80.
(26) Schewe, T.; Wiesner, R.; Rapoport, S. M. *Methods Enzymol.* **1981**, *71*, 430.
(27) Aasa, R.; Vänngård, T. *J. Magn. Reson.* **1975**, *19*, 308.
(28) SIM 15 was obtained from Quantum Chemistry Program Exchange.
(29) This $g = 6$ signal varies with protein preparation and appears to be correlated with the typical 410-nm absorption due to the heme Soret band. The $g = 6$ intensity does not change upon the addition of 13-HPOD, in contrast to the other EPR signals.

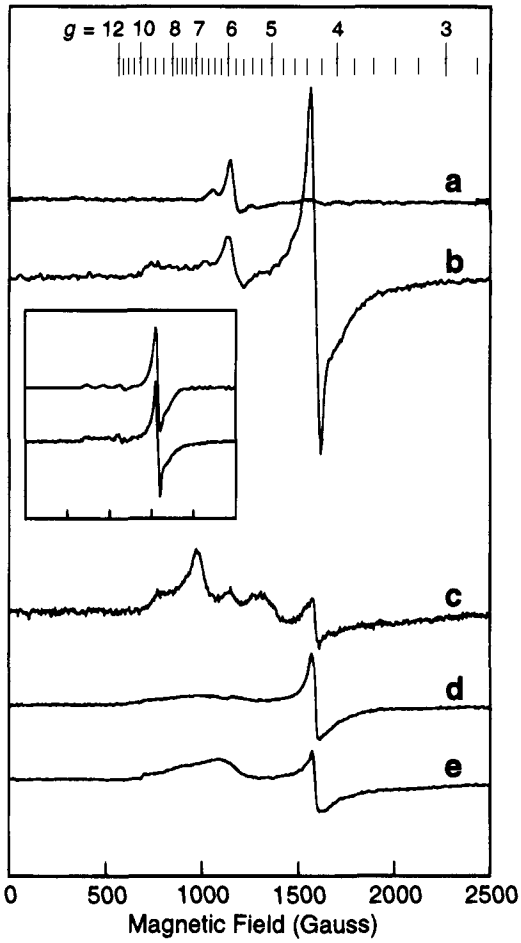

Figure 1. Low-temperature (7 K) EPR spectra of 15-RLO and 15-HLO: (a) resting ferrous 15-RLO (20.8 mg/mL) in 10 mM bis-Tris, 0.2 M NaCl, pH = 6.8 buffer; (b) 15-RLO sample from spectrum a treated with 1.1 equiv of 13-HPOD; (c) 15-RLO sample from spectrum b after the addition of 1.5 equiv more of 13-HPOD; (d) 15-HLO (17 mg/mL, in 20 mM phosphate, 0.2 M NaCl, pH = 7.0 buffer) treated with 1.3 equiv of 13-HPOD; and (e) 15-HLO sample from spectrum d after the addition of 2 equiv more of 13-HPOD. Inset: Ferric 15-RLO EPR spectrum obtained by subtracting spectrum a from spectrum b (bottom) and its simulation (top).

15-RLO with the addition of 1.1 equiv of 13-HPOD (Figure 1b) shows a large $g = 4.3$ signal and an additional weak signal at $g \approx 9.5$. This EPR pattern is characteristic of a high-spin ferric center with rhombic site symmetry (estimated $|E/D| = 0.32$) which is in sharp contrast to those of SLO-1 and 5-HLO ($|E/D| \approx 0$).[30] The growth of the $g = 4.3$ EPR signal of 15-RLO is accompanied by an increase in absorption intensity at 350 nm ($\epsilon = 3000\ M^{-1}\ cm^{-1}$, Figure 2b) relative to the absorption spectrum of the native ferrous enzyme (Figure 2a). This increased intensity at 350 nm is similar to the absorption behavior of ferric SLO-1[20] and 5-HLO,[21] for which this band has been assigned as a His→Fe^{3+} charge transfer transition.[18]

To determine the amount of EPR-visible iron in oxidized 15-RLO samples, ferric EDTA was used as a standard for spin quantitation since it also exhibits an EPR signal at $g = 4.3$. The EPR spectra of ferric 15-RLO and ferric EDTA taken under the same conditions were double integrated in the range of 0−3000 G (eliminating an impurity contribution at $g = 2$). The ratio obtained was used directly to estimate EPR-active iron as

(30) There is a small feature in the $g = 2$ region due to Mn contamination (not shown). It should be noted that the EPR intensity in the $g = 7$ region also increases with the addition of ~1.1−1.3 equiv of product and appears to arise from a fraction of oxidized sites which also have product bound (*vide infra*).

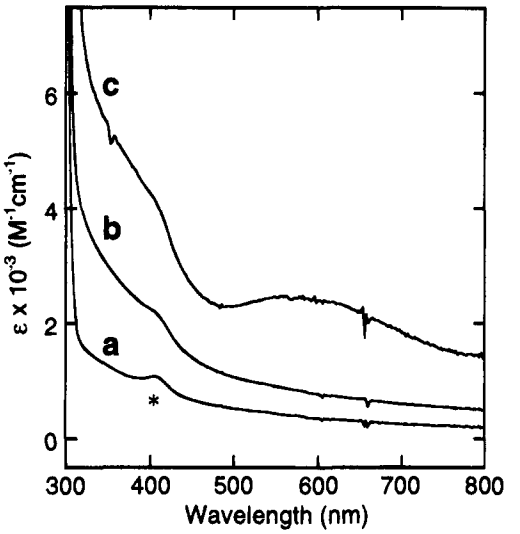

Figure 2. Room temperature absorption spectra of (a) ferrous 15-RLO, (b) ferrous 15-RLO treated with 1.1 equiv of 13-HPOD, and (c) ferrous 15-RLO treated with 2.5 equiv of 13-HPOD. (The asterisk indicates a contribution from a heme impurity.)

the EPR spectra of both samples exhibit a similar temperature dependence. From these quantitations it was determined that 80 ± 10% of the iron in 15-RLO + 1.2 equiv of 13-HPOD is EPR active.

Quantitation of the axial and rhombic EPR signal of 15-RLO is complicated by the fact that these two signals are spread over a large range, overlap, and have multiple components. These problems can be overcome by EPR simulations,[21,27,31,32] which were used to quantitate the spin population of signals in the rhombic and axial regions. The EPR spectrum of ferric 15-RLO, with the ferrous 15-RLO background subtracted out, and its simulation[33] are shown in the inset of Figure 1. Because there are multiple components in both the axial and rhombic regions, two axial doublets and three $g \approx 4.3$ rhombic doublets, plus an additional anisotropic lower doublet for the rhombic species, were required for the simulation. The relative weights used in the simulation reflect the relative populations of the EPR-active species present. To account for the spin population of all three M_S doublets, the temperature dependence of the axial and rhombic signals was measured to obtain the ZFS parameters. For the axial species, the average ZFS was determined to be $D = 0.3 \pm 0.2\ cm^{-1}$. For the rhombic $g = 4.3$ signal, the energy difference between doublets (Z) is $3.5 \pm 0.7\ cm^{-1}$, giving $|D| \approx 1.0\ cm^{-1}$. These ZFS parameters were used to calculate the Boltzmann population distributions of the three doublets, and the spin population was corrected accordingly. It was determined that the rhombic signal accounts for 75 ± 15% of the total EPR-active iron and that the axial signal accounts for 25 ± 15% of the total population. This rhombic-to-axial ratio is also produced by the double integration of the spectra obtained by subtracting out the axial and rhombic simulations, respectively.

When 1.5 equiv more of 13-HPOD is added to oxidized 15-RLO, the sample turns purple, similar to the behavior

(31) Slappendel, S.; Veldink, G. A.; Vliegenthart, J. F. G.; Aasa, R.; Malmström, B. G. *Biochim. Biophys. Acta* **1981**, *667*, 77.

(32) Gaffney, B. J.; Mavrophilipos, D. V.; Doctor, K. S. *Biophys. J.* **1993**, *64*, 773.

(33) EPR simulation parameters (unnormalized weight; g_z, width; g_x, width; g_y, width): iron #1 (30.0; 2.0, 30.0; 6.0, 90.0; 6.0, 90.0); iron #2 (180.0; 1.88, 30.0; 4.55, 100.0; 7.33, 100.0); iron #3 (50.0; 4.297, 55.0; 4.297, 55.0; 4.297, 55.0); iron #4 (50.0; 4.41,120.0; 4.15, 180.0; 4.27, 60.0); iron #5 (80.0; 4.30, 300.0; 4.30, 300.0; 4.30, 300.0); iron #6 (750.0; 1.03, 20.0; 1.64, 30.0; 9.20, 70.0). The simulation shown is not necessarily unique.

observed for SLO-1. This purple color gradually decays at both 4 °C and room temperature ($t_{1/2} \approx 5$ min). The EPR spectrum of the purple form of 15-RLO (Figure 1c) exhibits new intense signals at $g = 7.2$ and 5.5 with a large reduction in the $g = 4.3$ signal relative to the 1:1 oxidized form (Figure 1b),[34] demonstrating that the rhombic ferric center has been converted to a nearly axial site with a small rhombic distortion, $|E/D| < 0.06$ based on spin Hamiltonian calculations. As shown in Figure 2c, this purple form is associated with an absorption band at ~580 nm ($\epsilon = 2400$ M^{-1} cm^{-1}), as has also been observed for SLO-1, indicating the same type of ferric–peroxide product interaction for both LOs.

The recombinant 15-HLO active site has also been studied using EPR and absorption spectroscopies. When treated with 1.3 equiv of 13-HPOD, ferrous 15-HLO turns yellow and exhibits an increase in absorption at 350 nm, consistent with other LOs. The EPR spectrum of this yellow form of 15-HLO (Figure 1d) exhibits a large signal at $g = 4.3$ and a weak signal at $g = 9.5$,[30] demonstrating that ferric 15-HLO, similar to ferric 15-RLO, has an active site with rhombic effective symmetry. Addition of a 2.0-fold further excess of 13-HPOD to the oxidized 15-HLO sample results in a darker solution, whose color disappears within seconds. The dark color is associated with the formation of a ferric enzyme–product complex similar to that observed for SLO-1 and 15-RLO. The EPR spectrum of this 15-HLO–product complex (Figure 1e) shows increased intensity in the $g = 6.6$ region and an intensity decrease of the $g = 4.3$ signal,[34] indicating that the ferric active site has been converted from rhombic to axial upon coordination of the 13-HPOD product. This EPR behavior is opposite to that observed for SLO-1 and 5-HLO, but it parallels the behavior of 15-RLO.

Discussion

From the EPR studies presented above, dramatic differences are observed between the ferric active sites of rabbit and human 15-LOs *vs* plant 15-LO and human 5-LO. The oxidation of native ferrous SLO-1 to the ferric form produces axial EPR signals in the $g \approx 6$ region. Addition of a 2-fold excess of the hydroperoxide product 13-HPOD converts the active site from *axial to rhombic* symmetry.[20] Alternatively, oxidation of rabbit and human 15-LOs results in a rhombic Fe^{3+} site with a $g = 4.3$ EPR signal.[35] Addition of a 2-fold excess of product to both ferric mammalian 15-LOs results in a purple complex with a new absorption band at 580 nm, which has also been observed for the product complex of SLO-1. The mammalian ferric 15-LO–product complex, however, exhibits an EPR signal in the $g \approx 6.0$ region, indicating that product coordination has caused the rabbit and human 15-LO sites to convert from *rhombic to axial* symmetry.

In earlier studies,[18,36] we have used variable-temperature MCD and EPR spectroscopies to obtain the ZFS parameters of non-heme ferric sites and have developed the ligand field origins of the ground-state ZFS based on the Griffith model.[37] This methodology can now be applied to the active sites in 15-RLO and 15-HLO (15-R/HLO to represent both mammalian enzymes) and to SLO-1 (as representative of both SLO-1 and 5-HLO) to correlate EPR behavior with active site structure. The ZFS parameters D and E of the $^6A_1$ ground state derive from spin–orbit coupling to a low-lying $^4T_1(t_2^4e^1)$ excited state which is split in energy due to the less than octahedral symmetry. D and E can be calculated from eqs 2 and 3,[18] respectively, where

Scheme 1

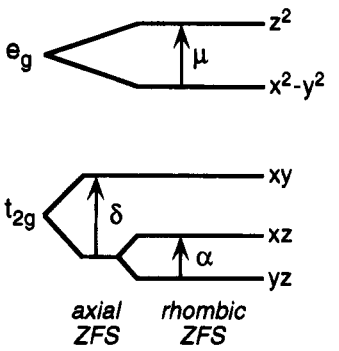

$$D = \frac{(\zeta_{Fe^{3+}})^2}{10}\left[\frac{2\kappa_z^2}{E(^4T_1(z))} - \frac{\kappa_y^2}{E(^4T_1(y))} - \frac{\kappa_x^2}{E(^4T_1(x))}\right] \quad (2)$$

$$E = \frac{(\zeta_{Fe^{3+}})^2}{10}\left[\frac{\kappa_y^2}{E(^4T_1(y))} - \frac{\kappa_x^2}{E(^4T_1(x))}\right] \quad (3)$$

$\zeta_{Fe^{3+}}$ is the one-electron spin–orbit coupling parameter for ferric iron ($\zeta_{Fe^{3+}} = 430$ cm^{-1}) and $E(^4T_1(i))$ are the energies of the orbital components of the low-symmetry split $^4T_1$ excited state which spin–orbit couples to the $^6A_1$ ground state. κ_i are reduction factors related to covalency and have been defined elsewhere.[18] Because anisotropic covalency was found to have limited effect on the ZFS parameters for distorted octahedral ferric complexes,[18] we treat the covalency as isotropic ($\kappa_x = \kappa_y = \kappa_z$). The energies of the $^4T_1(i)$ orbital components for octahedral or square-pyramidal complexes are given by eq 4.[18]

$$E(^4T_1(x)) = E(^4T_1(\text{cubic})) + \frac{1}{3}\left(\delta + \frac{3}{4}\mu + \frac{3}{2}\alpha\right) \quad (4a)$$

$$E(^4T_1(y)) = E(^4T_1(\text{cubic})) + \frac{1}{3}\left(\delta + \frac{3}{4}\mu - \frac{3}{2}\alpha\right) \quad (4b)$$

$$E(^4T_1(z)) = E(^4T_1(\text{cubic})) - \frac{2}{3}\left(\delta + \frac{3}{4}\mu\right) \quad (4c)$$

$E(^4T_1(\text{cubic}))$ is the average energy of the transition from the $^6A_1$ ground state to the low-lying $^4T_1$ excited state (due to the octahedral ligand field plus electron repulsion) and has been estimated to be ~7200–11 400 cm^{-1} for distorted octahedral ferric sites.[18] The $^4T_1(i)$ energies depend on the one-electron d-orbital splittings through the parameters δ, μ, and α, which are defined as $\delta = (E(d_{xz}) - E(d_{yz}))/2 - E(d_{xy})$, $\mu = E(d_{x^2-y^2}) - E(d_{z^2})$, and $\alpha = E(d_{yz}) - E(d_{xz})$ and are depicted in Scheme 1. Thus, given the d-orbital energies under a specific ligand field and the average $^6A_1 \rightarrow {}^4T_1$ transition energy, the ZFS parameters D and E can be calculated for a given ferric site.

The LF model developed by Companion and Komarynsky[38] was used to obtain the one-electron d-orbital energy splitting for ferric SLO-1, ferric 15-R/HLO, and their product-bound (purple) forms. The four idealized LO sites shown in Figure 3

(34) Note that the purple form of lipoxygenase is unstable and that the EPR intensity distribution between rhombic and axial signals varies depending on the amount of product used and the time of freezing after the addition of product, and from purification to purification.

(35) There have been two reports on the EPR spectra of rabbit lipoxygenase which suggest that ferric 15-RLO exhibits multicomponent EPR features in the axial $g = 6$ region similar to those of SLO-1 and 5-HLO (Boyington *et al. Ann. N.Y. Acad. Sci.* **1995**, *744*, 310. Carroll *et al. Lipids* **1993**, *28*, 241). In these two studies, the ferric 15-RLO sample may have been partially converted to its purple form, which has an axial EPR signal.

(36) Gebhard, M. S.; Deaton, J. C.; Koch, S. A.; Millar, M.; Solomon, E. I. *J. Am. Chem. Soc.* **1990**, *112*, 2217.

(37) Griffith, J. S. *Mol. Phys.* **1964**, *8*, 213.

(38) Companion, A. L.; Komarynsky, M. A. *J. Chem. Educ.* **1964**, *41*, 257.

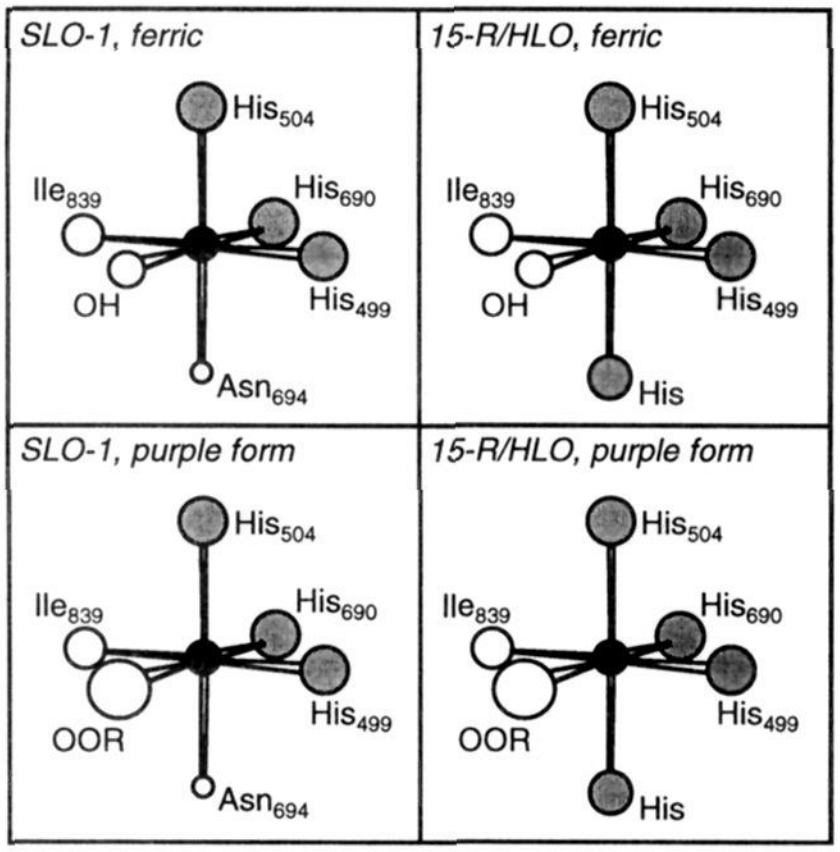

Figure 3. Iron active site coordination models of SLO-1 (left) relative to rabbit and human 15-LOs (right) based on spectroscopic studies,[2,3,5,7] crystal structures,[8,9] and amino acid sequence comparisons.[16,17] The iron is represented as a black ball, nitrogen ligands as shaded balls, and oxygen ligands as white balls; the size of the ligands indicates their proposed relative LF strengths (larger balls for stronger ligand fields).

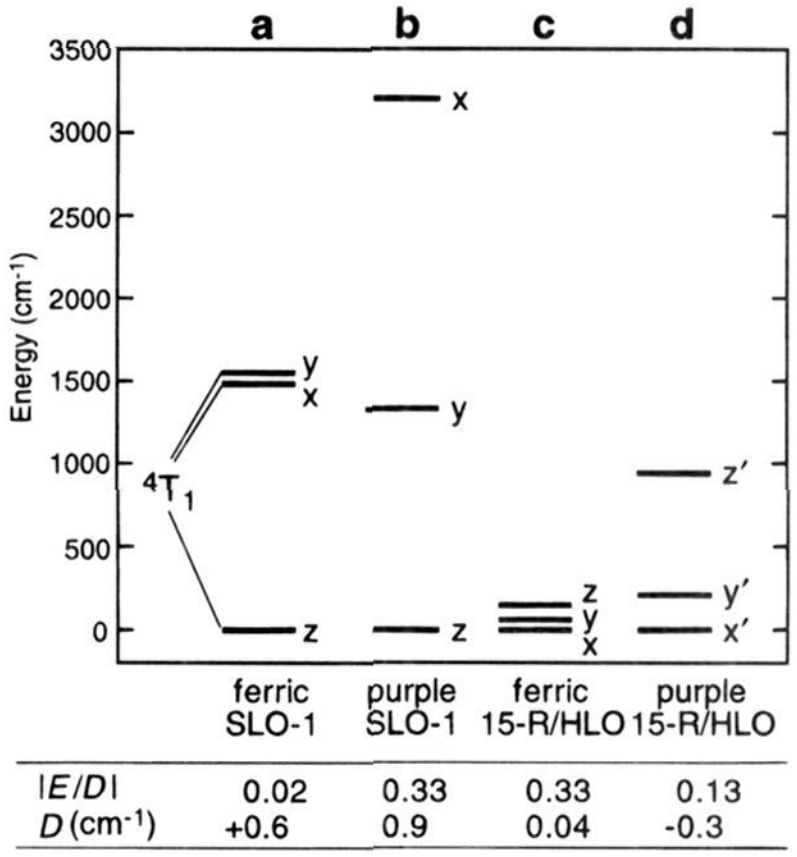

	ferric SLO-1	purple SLO-1	ferric 15-R/HLO	purple 15-R/HLO
$\|E/D\|$	0.02	0.33	0.33	0.13
D (cm^{-1})	+0.6	0.9	0.04	-0.3

Figure 4. Calculated energies of the $^4T_1(x,y,z)$ orbital components, $|E/D|$ ratios, and D values for (a) ferric SLO-1, (b) the purple (*i.e.*, product-bound) form of SLO-1, (c) ferric 15-R/HLO, and (d) the purple form of 15-R/HLO. The z-axis is defined along the Asn_{694}/His−Fe−His_{504} direction for a−c and along the ROO−Fe−His_{690} direction for d (see Figure 3). The SLO-1 product−enzyme complex (b) and ferric 15-R/HLO (c) are at the rhombic limit; therefore, no sign is given for the ZFS.

are based on spectroscopic studies,[2,3,5,7] crystallographic information,[8,9] and amino acid sequence comparisons.[16,17] LF calculations were performed by treating the more covalent ligands, such as histidine, as strong-field ligands and varying the LF strengths of the other ligands accordingly. The d-orbital energies obtained from these calculations are inserted into eq 4 to obtain the $^4T_1$ component energies, which then give the ZFS parameters D and E through eqs 2 and 3. Figure 4 shows the resulting $^4T_1(i)$ energies, D values, and $|E/D|$ ratios for each of the four LO sites in Figure 3.[39]

In agreement with experimental EPR results,[18,20] these calculations predict an axial site ($|E/D| = 0.02$) and a positive D for ferric SLO-1. This axial symmetry arises from the asparagine ligand being a very weak-field ligand, creating a weak tetragonal axis along the Asn_{694}−Fe−His_{504} direction (defined as the z-axis) and C_{4v} effective site symmetry[40] (Figure 3, upper left). Evidence for a weak asparagine bond comes from the ferrous SLO-1 crystallographic studies which show this residue as either bound to the metal with a long bond length[9,10] or not bound at all.[8] The weak z-axis causes a large splitting of the $^4T_1(z)$ from the $^4T_1(x,y)$ components and overcomes small ligand field differences in the xy-plane so that the d_{xz} and d_{yz} orbitals are not very split (small α). This causes the $^4T_1(x)$ and $^4T_1(y)$ to be relatively close in energy and produces a small $|E/D|$ ratio (see Figure 4a).[41] The positive value for D arises from the d_{z^2} orbital being lower in energy than the $d_{x^2-y^2}$ orbital.[18] Product coordination to produce the purple form of SLO-1 results in an additional covalent ligand (based on the low-energy product→Fe^{3+} charge transfer transition) *trans* to one of the histidines, which lowers the effective site symmetry to C_{2v}. This is shown in Figure 3, lower left, where the hydroxide has been replaced with an alkylperoxide group. The LF strength of ROO^- is expected to be much stronger than Ile in the xy-plane (where z is still defined along the Asn_{694}−Fe−His_{504} direction) and thus induces a rhombic distortion on the tetragonal site. In this case, the d_{xz} and d_{yz} orbitals are split by a large amount (large α), and the $^4T_1(x)$ and $^4T_1(y)$ levels are no longer close in energy, producing a rhombic site with $|E/D| = 0.33$, as shown in Figure 4b. The value of D obtained for the purple form of SLO-1 is on the order of that calculated for the ferric enzyme, in agreement with EPR results.[18,20]

Correlating SLO-1 to 15-R/HLO, the asparagine ligand is substituted for a histidine in the amino acid sequence.[16,17] The histidine substitution would put a more covalent ligand in place of the weak-field asparagine ligand (Figure 3, upper right). The new His ligand should have a LF strength stronger than, but comparable to, those of Ile and OH in the xy-plane, keeping z defined along the Fe−His_{504} bond. Similar LF strengths along x, y, and z produce a rhombic site with C_{2v} effective symmetry. The calculations show that the $^4T_1(i)$ energies are equally spaced (Figure 4c), giving $|E/D| = 0.33$, and that D is reduced relative to that of ferric SLO-1, in qualitative agreement with experimental results. Coordination of the hydroperoxide product results in a complex with five strongly covalent ligands (Figure 3, lower right). The new ROO^- ligand should have a stronger LF strength than the other ligands and produce a strong

(39) Ligand field parameters (α_2, α_4) (cm^{-1}) for d-orbital energy calculations: $His_{499,504,690}$ (19200, 6400), Ile_{839} (16704, 5568), OH (16512, 5504), Asn_{694} soybean (5760, 1920), His mammalian (17280, 5760), ROO^- soybean (22080, 7360) and mammalian (23040, 7680). The x-, y-, and z-axes were defined along the His_{499}, His_{690}, and His_{504} directions using a right-handed coordinate system. Parameters for ZFS calculations: $E(^4T_1\text{-(cubic)}) = 9000\ cm^{-1}$, $\zeta = 430\ cm^{-1}$, and $\kappa^2 = 0.81$.

(40) We use the term "effective symmetry" to indicate that although the protein sites have low rigorous symmetry, they are close to higher effective symmetry models which allow additional insight. For example, while the upper left structure in Figure 3 has C_1 rigorous symmetry, the fact that the Asn has a very weak ligand field relative to the other ligands results in a site with approximately C_{4v} symmetry, indicating an axial system.

(41) In the calculations shown, Asn_{694} was given 30% of the LF strength of the three conserved His ligands; however, an axial site is also predicted for asparagine LF strengths up to 70% of the histidine LF strength. Removal of this asparagine ligand altogether still results in a unique weak direction along the Fe−His_{504} bond.

tetragonal axis along the ROO−Fe−His_{690} direction (now defining a new z-axis) to give C_{4v} effective symmetry. This arrangement results in a more axial site, $|E/D| = 0.13$ (see Figure 4d), which is consistent with the EPR changes. Note that although the value of D for the product-bound forms of 15-R/HLO was not explicitly determined from the EPR data, the calculations indicate a negative D since d_{z^2} is higher in energy than $d_{x^2-y^2}$[18] for the strong axial alkylperoxide system.

It is surprising to find an axial site in a non-heme iron center because of the mixed ligation and low symmetry of such systems. However, the above calculations provide insight into the axial symmetry found for ferric SLO-1, showing that it is the result of a unique weak-field direction, associated with a long, weak Asn bond, which overcomes other smaller LF differences. Substitution of this asparagine (Asn_{694}) with histidine makes all ligands similar to each other in a low-symmetry site and logically produces a rhombic system for 15-RLO and 15-HLO. The SLO-1 hydroperoxide product−enzyme complex exhibits an intense low-energy charge transfer transition, indicating a covalent ligand with a strong ligand field. The combination of this strong ROO^- ligand with the weak Asn ligand produces a rhombic site for the SLO-1 product−enzyme complex. For the hydroperoxide product−enzyme complexes of 15-RLO and 15-HLO, the ROO^- ligand creates a unique strong direction which overcomes other small symmetry differences and results in a more axial site. Thus, these results are consistent with an Asn_{694}→His substitution in the rabbit and human 15-LOs and the hydroperoxide product forming a reasonably strong covalent bond to the iron site.

While the above LF structural model of the active sites and the absorption spectra of purple 15-RLO and SLO-1 suggest the same mode of product coordination to the iron for plant and mammalian LOs, mechanistic similarities are also implied as the ferric enzyme−product complex has been proposed to be an intermediate in the reaction mechanism.[42] However, since histidine is a much stronger ligand and a better electron donor to the iron center, the Asn_{694}→His substitution should lower the redox potential and thus stabilize the ferric oxidation state of the active site in rabbit and human 15-LOs relative to SLO-1. If reduction of the ferric enzyme is required for catalysis as has been suggested in some proposed mechanisms,[42] the stability of ferric 15-R/HLO would lower the activity of the mammalian enzymes relative to SLO-1. In fact, 15-RLO and 15-HLO have comparable K_m values, but lower V_{max} values relative to those of SLO-1,[26,43,44] consistent with the increased stability of the 15-R/HLO ferric sites which would occur due to His substitution. Asn_{694}→His SLO-1 and the corresponding His→Asn human 15-LO mutants are presently being explored to systematically investigate the geometric and electronic structure differences described above and their relation to reactivity.[45]

Acknowledgment. This work was funded by the National Institutes of Health (Grant No. GM40392, E.I. S., and HL48591, E. S.). We are grateful to Dr. Jim Barnett of Syntex Discovery Research for the preparation of human recombinant 15-LO. Y.Z. gratefully acknowledges Dr. Harold Van Wart, Director of the Institute of Biochemistry and Cell Biology at Syntex, for providing the opportunity and generous support for her work on this project. We also thank Mark Pavlosky of Stanford for his assistance in preparation of this manuscript.

JA943114H

(42) Nelson, M. J.; Cowling, R. A.; Seitz, S. P. *Biochemistry* **1994**, *33*, 4966.

(43) Axelrod, B.; Cheesbrough, T. M.; Laakso, S. *Methods Enzymol.* **1981**, *71*, 441.

(44) Sloane, D. L.; Leung, R.; Barnett, J.; Craik, C. S.; Sigal, E. *Protein Eng.* **1995**, in press.

(45) Recently, the Asn_{694}→His mutant has been prepared for SLO-1 (Holman, T.; Axelrod, B.; Sigal, E.; Solomon, E. I., unpublished results) as well as SLO-3 (Kramer *et al. Biochemistry* **1994**, *33*, 15017). The spectral properties of this mutant at suitable protein concentrations for good EPR signal-to-noise ratios are presently being determined.